



ChemComm

**Acoustic Levitation and Infrared Thermography: A Sound Approach to Studying Droplet Evaporation**

Journal:	<i>ChemComm</i>
Manuscript ID	CC-COM-12-2019-009856.R2
Article Type:	Communication

SCHOLARONE™  
Manuscripts

## COMMUNICATION

## Acoustic levitation and infrared thermography: A sound approach to studying droplet evaporation

Received 00th January 20xx,  
Accepted 00th January 20xx

DOI: 10.1039/x0xx00000x

Edward R. Duranty\*, Harley McCardle, W. Matthew Reichert, James H. Davis, Jr.

**Herein we report a new technique combining acoustic levitation and infrared thermography to directly monitor droplet surface temperatures. Using it, temperature profiles were recorded during the evaporation of deionized water, methanol, *n*-propanol, and isopropanol. Results support the viability of this inexpensive and easily-accessed technique for studying chemical and physical changes in droplets.**

Small volume chemistry has become of interest recently, especially since the first reports of increased reaction rates within various small volume containers - including microfluidic systems<sup>1,2</sup>, thin films on surfaces<sup>3,4</sup>, and in droplets<sup>5-8</sup> - were published. There have been many recent examples in the literature of this phenomenon in aqueous droplets and micro-droplets involving simple bimolecular acid-catalyzed reactions<sup>9</sup>, various syntheses<sup>10-12</sup>, and even in more complex processes such as protein unfolding<sup>13</sup>. These studies attribute the increase in observed rates of reaction to two key parameters inherent to small containers: increased surface area<sup>8</sup> and rapid mixing times within the small volume<sup>11,13</sup>. In the present work, these important characteristics are leveraged to study the thermodynamics of evaporation of water and three different but chemically similar organic solvent droplets in order to better understand their behavior when they are part of the matrix of an organic aerosol.

Organic solvent droplets are commonly generated in the laboratory using spray methods which act as ionization methods in mass spectrometry. These methods include electrospray<sup>9,14</sup>, paper spray<sup>15</sup>, electrostatic levitation<sup>16</sup>, magnetic levitation<sup>17</sup>, and the less common ambient ionization via acoustic levitation<sup>18</sup>. In the latter method, sample droplets are levitated using standing acoustic (or sound) waves, thereby

isolating a small volume droplet ranging from nanoliters to microliters in volume in an ambient atmosphere. Acoustic levitation results in a “contact-free” container, meaning that the sample is contained within a localized space without the use of a sample holder or cuvette.<sup>19</sup> As a result, the surface of the droplet remains free for chemical activity and heat transfer directly to and from the surrounding atmosphere. These features make acoustic levitation of droplets an attractive and (given the quite low equipment costs involved) readily accessible option for use in studying processes dependent on the flow of heat and material across the droplet/air interface such as evaporation.

In this communication we demonstrate that unique insights can be gained by combining an acoustic levitation-based methodology with infrared thermography, as seen in Figure 1, to monitor the surface temperature of organic solvent droplets. The organic compounds chosen for this study include methanol and two structural conformers *n*-propanol and isopropanol, all of which have been reported to be present in the atmosphere. The work presented here uses this new technique to shed light on the thermodynamics of the evaporation process these organic solvents undergo in suspended droplet form. These results, characteristic of acoustic levitation combined with thermography, demonstrate the viability of the technique and should prove useful in fields such as atmospheric aerosols<sup>20</sup> and aerosol reactors<sup>21</sup>.

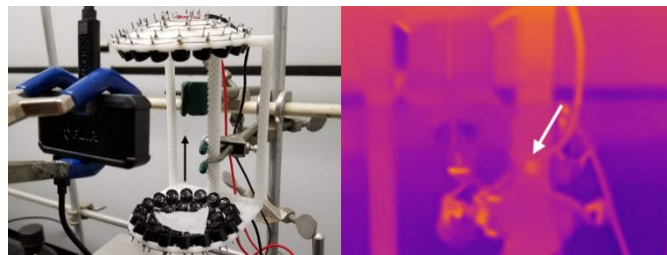


Figure 1: (Left) TinyLev apparatus levitating a liquid sample indicated by the black arrow while monitored by the FLIR One Pro camera. (Right) Representative thermal image of levitating drop, indicated by the white arrow, obtained from the FLIR One Pro camera.

<sup>a</sup> University of South Alabama, Department of Chemistry, 6040 USA South Drive, Mobile, AL 36688

Electronic Supplementary Information (ESI) available: Evaporation profile regression curves, long term (>650 s) evaporation profiles. See DOI: 10.1039/x0xx00000x

As mentioned, the organic solvents used in this work include *n*-propanol, isopropanol, and methanol. Droplets of these solvents, as well as deionized water, were levitated using a "TinyLev" acoustic levitator<sup>19</sup> that was assembled from a commercially available kit and was similar in design to the devices used in our group's previous studies.<sup>22</sup> The TinyLev generates a standing acoustic wave via two parallel transducer arrays mounted on a 3D printed polylactic acid (PLA) scaffolding. The transducers are driven by a L298N dual motor driver and powered by a 9-12V AC power supply. The 40 kHz signal output from the transducer arrays was generated using an Arduino Nano microcontroller. After assembly, the device was powered on and a small (~2-5  $\mu\text{L}$ ) droplet of solvent was injected into one of the nodes near the center of the standing wave using a 25  $\mu\text{L}$  gas chromatography (GC) syringe.

In the acoustic levitator, the droplet is supported by a maximum in the standing acoustic wave. The sound produced by the parallel arrays of transducers making up the TinyLev generate a series of alternating constructive and destructive areas of sound within the volume of space between them. As sound propagates as a pressure wave, these areas of constructive and destructive interference result in alternative areas of greater and lesser density in the gas medium between the transducer arrays. It is into the areas of lower density, which are nodes in the standing acoustic wave, that the solvent samples are injected using the GC syringe. The solvent injected into the node forms into a droplet and rests on the area of higher density immediately below the node.

Once a droplet was successfully isolated within the standing

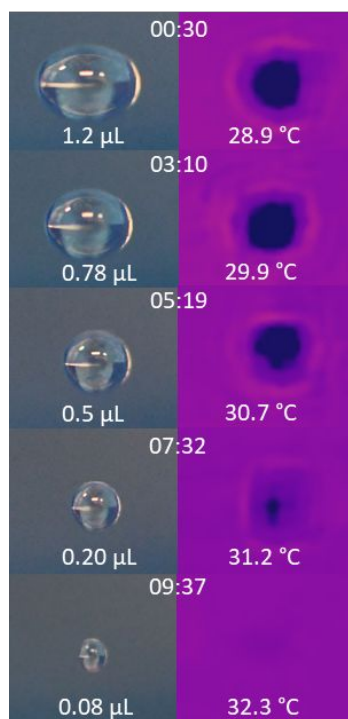


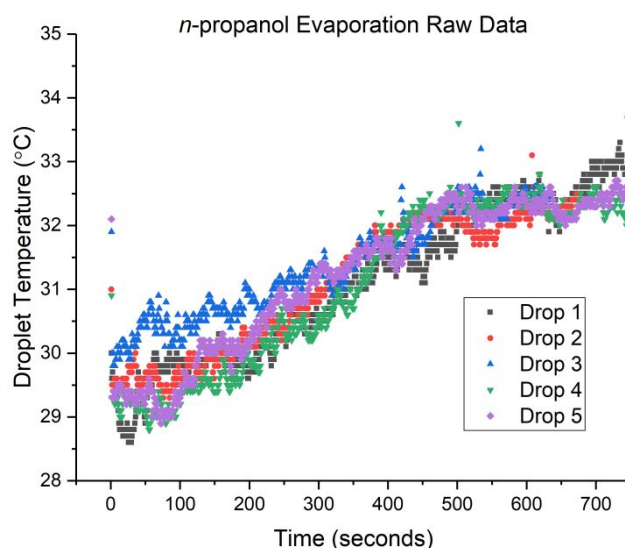
**Figure 2:** Time-lapse visible images and IR thermographs of the evaporation of an *n*-propanol droplet. Visible images were taken with a Nikon D7500 DSLR camera using a Nikon Nikkor AF-S DX 85mm f/3.5G ED VR fixed zoom lens while thermographic images were captured using the FLIR One Pro IR camera.

2 | *Journal Name*, 2012, 00, 1-5

acoustic wave, a FLIR® One Pro thermographic camera was used to monitor the surface temperature of the levitating droplet during evaporation. The forward-looking infrared (FLIR) camera thermal sensor in the FLIR ONE Pro has a resolution of 160 x 120 pixels with a pixel size of 12  $\mu\text{m}$  and a 8 – 14  $\mu\text{m}$  spectral range. This sensor is capable of measuring temperatures between -20°C and 400°C with an accuracy of  $\pm 5\%$ . The default emissivity value 0.90 was used for our samples which has been reported as a common value for water.<sup>23</sup> The camera was controlled using the FLIR Tools application on a Lenovo TAB2 A10 tablet running Android 6.0. Using a

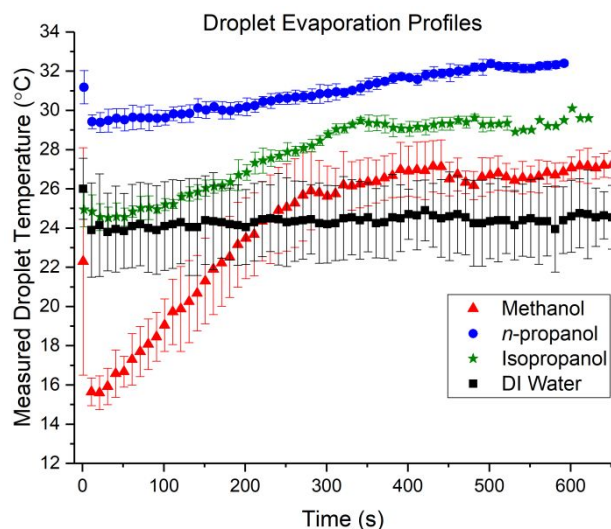
preview thermographic image of the droplet generated by the FLIR Tools software, a point within the droplet was selected for monitoring. The software then sampled the camera's sensor at that point each second and droplet surface temperature data for each liquid studied was collected until droplet evaporation was complete. Under the same conditions this process was repeated five times for each solvent studied excluding water, data for which was collected only twice due to the long droplet persistence lifetimes as compared to the alcohols. A characteristic time-lapse demonstrating the change in droplet size due to evaporation is seen for an *n*-propanol droplet in Figure 2. The images in the left column were captured at the given time using a Nikon DSLR camera and a 1:1 macro lens while the thermographic images in the left-hand column were simultaneously captured using the FLIR One IR camera. The FLIR One Pro camera used has a fixed focal length of 15 cm, so as a result the droplet thermograms are not completely in focus, as seen by the "haze" around the droplets on the right-hand side of Figure 2. Droplet volumes reported in Figure 2 were calculated droplet diameters measured using ImageJ<sup>24</sup> based on the 5568x3712 pixel, 23.4x15.6 mm sensor of the Nikon D7500 and assuming the droplets formed an ellipsoid.

Figure 3 contains characteristic raw data obtained from the FLIR camera, in this case for *n*-propanol. The average temperature profiles for the organic solvent droplets during the evaporation process are displayed in Figure 4, along with that from water. It is apparent from these data that the three relatively similar organic solvent droplets studied here seem to have uniquely different evaporation behavior in the first 500 seconds after deposition. All three of the alcohol droplets evaporate rather quickly as compared to the deionized water droplet, and each exhibits a drop in temperature immediately after deposition into the acoustic node. The most obvious commonality between the four solvents is the initial decrease in temperature due to evaporative cooling followed by an increase to some final temperature where the data plateau. This plateau represents the complete evaporation of the droplet, at which point the FLIR camera is only measuring the ambient temperature. It should be noted that while each set of data for a given solvent was collected on the same day, the ambient temperature did change



This journal is © The Royal Society of Chemistry 20xx  
**Figure 3:** Raw *n*-propanol evaporation profiles for the five droplets studied.

from day to day resulting in the differing values of the temperature plateau in the data from Figure 4.



**Figure 2:** Short time-scale (below 1000 seconds) average droplet temperature averages with error for methanol (red triangles), *n*-propanol (blue circles), isopropanol (green stars), and deionized water (black squares).

While the temperature profiles for the studied organic solvents bear the same general trend, an initial decrease followed by an increase in temperature, the rate at which both of these temperature changes occur are drastically different. The initial temperature drop for the heavier alcohols was relatively slight, at approximately 2°C for the *n*-propanol and 0.5°C for the isopropanol droplet respectively, and occurred over the course of approximately a minute. This trend is similar to the one seen in deionized water which dropped about 2°C immediately following deposition. However the lighter alcohol methanol exhibited a very large 7°C drop occurring very quickly within the first few seconds of droplet deposition into the acoustic node.

**Table 1:** Linear regression results for solvent droplet temperatures after deposition.

Solvent	DI Water	Methanol	<i>n</i> -propanol	Isopropanol
Increase Rate (°C/s)	0.19E-3 ±8.1E-6	4.13E-2 ±2.0E-4	0.65E-2 ±4.4E-5	1.78E-2 ±8.63E-5
Rate Relative to Methanol	4.60%	100%	15.7%	43.1%
R-squared Parameter	0.95	0.99	0.98	0.99

However, the most striking difference in the droplet evaporation profiles is the rate of increase in temperature after the temperature decreased following droplet deposition. Since the increase in each of these seemed to be linear, the temperature data from the minimum value to the beginning of the plateau were fit using a linear model, the data for which is presented in Table 1. These data seem to agree with the initial visual inspection of the solvent temperature profiles with methanol increasing in temperature the fastest at 4.13E-2 °C/s.

The remaining solvent increased in temperature at a significantly slower rate where the other two alcohols

isopropanol and *n*-propanol are heating at 43.1% and 15.7% of the rate of methanol respectively. The slowest heating solvent studied was the deionized water droplet which heated at only 4.60% of the rate of the methanol droplet.

In general, these rates follow the expected trends based on visual inspection of Figure 4. Deionized water has a very slow heating rate, almost two orders of magnitude slower than methanol, which heats the most quickly. Meanwhile the two propanol conformers feature similar rates with isopropanol heating approximately twice the rate of *n*-propanol. Based on these measured heating rates, one would expect the water droplet to have the highest value of the molar enthalpy of vaporization ( $\Delta H_{vap}$ ) since it heats the slowest and persists in the field for the longest amount of time. However, this trend does not match  $\Delta H_{vap}$  values described in the literature, where water is reported to have a value of 43.8 kJ/mol<sup>25</sup>, and *n*-propanol and isopropanol have values of 46.7 and 45.5 kJ/mol respectively.<sup>26</sup> Only methanol has a lower  $\Delta H_{vap}$  (37.0 kJ/mol<sup>27</sup>) than that of water. As a result, the droplet heating rates measured in this work *do not* correlate with only values of  $\Delta H_{vap}$  and suggest that the heating, and resulting evaporation, of droplets suspended in the acoustic field is not a single parameter-dependent process and is instead driven by a more complex multivariate mechanism.

Interestingly, such multivariate mechanisms have been suggested in the literature<sup>28</sup> and have been applied to electrospray-generated droplet formation in mass spectrometry-based ionization sources.<sup>29</sup> In short, two different mechanisms for droplet evaporation have been proposed based on the size of the droplet: a mechanism where the rate of evaporation is dependent on molecules escaping a gaseous layer surrounding the droplet; and a second where the rate becomes dependent on primarily on the  $\Delta H_{vap}$  and surface area of the droplet.<sup>30</sup> The first mechanism is usually associated with large droplets with a radius above some critical value (~0.10 μm for methanol, for example)<sup>29</sup>, at which the formation of a vapor layer immediately above the surface of the droplet is enabled. In this mechanism, called diffusion-controlled evaporation, the escape of a solvent molecule into the atmosphere is controlled by the rate of change in the density of this vapor layer. The second evaporation mechanism is referred to as surface-controlled evaporation where the rate of evaporation is dependent on the chemical nature of the solvent, explicitly  $\Delta H_{vap}$ , and the number of molecules exposed to the atmosphere at the surface of the droplet.

It is not completely clear from the data in Figure 4 and Table 1 which mechanism is controlling the evaporation of the acoustically-levitated solvent droplets. More data will be required in order to study the evaporation mechanism of these droplets, including a study of the effects of molar volume by analyzing bulkier alcohols such as *n*-butanol and *tert*-butanol, the role of ambient humidity, and the effects of possible energy transfer to the droplet from the acoustic field itself. These experiments will likely require isolation of the measurement

device in a dry, controlled-atmosphere glovebox, to which we are currently working to gain access.

In closing, we show that from a methodological point of view, a readily-available parallel array of 40 kHz transducers can be used to levitate a small volume of solvent within a node of a standing acoustic wave. In conjunction with an FLIR thermographic camera interfaced with an Android tablet, the approach allows for a rather inexpensive (especially compared to existing approaches) and direct real-time monitoring of solvent liquid droplet's surface temperature during the process of evaporation separate from the bulk.

From the standpoint of presently observed evaporative behaviors, the results in Figure 3 suggest that the evaporation of liquid droplets is not driven simply by the material's enthalpy of vaporization, but is instead driven by a complex mechanism dependent on the size of the droplet in conjunction with the chemical identity of the solvent. This conclusion agrees with previous experiments reported in the literature that have studied the process of droplet evaporation that were measured indirectly using complex, and quite costly, volatilization sources. While more work is required to determine which of the aforementioned evaporation mechanisms is operative in acoustically-levitated droplets, this preliminary study demonstrates the viability of a combined acoustic levitation/thermography methodology for studying their thermodynamic behavior. This, in turn, has practical ramifications for studying the dynamic behavior of aerosols ranging from those naturally occurring in the environment, to the use of spray-drying in pharmaceutical processing, and even to the behavior of paints and coatings being spray-applied to substrates.

### Conflicts of interest

There are no conflicts to declare.

### Notes and references

‡ The authors would like to acknowledge the University of South Alabama's Faculty Development Council for supporting this project. JHD thanks the National Science Foundation for partial support of this work under grant number CHE-1464740.

- H. Song, D. L. Chen and R. F. Ismagilov, *Angew. Chemie - Int. Ed.*, 2006, **45**, 7336–7356.
- C. G. Yang, Z. R. Xu and J. H. Wang, *TrAC - Trends Anal. Chem.*, 2010, **29**, 141–157.
- C. S. Lee, W. Yin, A. P. Holt, J. R. Sangoro, A. P. Sokolov and M. D. Dadmun, *Adv. Funct. Mater.*, 2015, **25**, 5848–5857.
- A. K. Badu-Tawiah, D. I. Campbell and R. G. Cooks, *J. Am. Soc. Mass Spectrom.*, 2012, **23**, 1461–1468.
- S. Narayan, J. Muldoon, M. G. Finn, V. V. Fokin, H. C. Kolb and K. B. Sharpless, *Angew. Chemie - Int. Ed.*, 2005, **44**, 3275–3279.
- D. C. Rideout and R. Breslow, *J. Am. Chem. Soc.*, 1980, **102**, 7816–7817.
- Y. Li, X. Yan and R. G. Cooks, *Angew. Chemie - Int. Ed.*, 2016, **55**, 3433–3437.
- R. M. Bain, S. Sathyamoorthi and R. N. Zare, *Angew. Chemie - Int. Ed.*, 2017, **56**, 15083–15087.
- M. Girod, E. Moyano, D. I. Campbell and R. G. Cooks, *Chem. Sci.*, 2011, **2**, 501–510.
- R. M. Bain, C. J. Pulliam and R. G. Cooks, *Chem. Sci.*, 2015, **6**, 397–401.
- J. K. Lee, S. Banerjee, H. G. Nam and R. N. Zare, *Q. Rev. Biophys.*, 2015, **48**, 437–444.
- A. Fallah-Araghi, K. Meguellati, J. C. Baret, A. El Harrak, T. Mangeat, M. Karplus, S. Ladame, C. M. Marques and A. D. Griffiths, *Phys. Rev. Lett.*, 2014, **112**, 1–5.
- J. K. Lee, S. Kim, H. G. Nam and R. N. Zare, *Proc. Natl. Acad. Sci.*, 2015, **112**, 3898–3903.
- R. M. Bain, C. J. Pulliam, F. Thery and R. G. Cooks, *Angew. Chemie - Int. Ed.*, 2016, **55**, 10478–10482.
- R. M. Bain, C. J. Pulliam, S. A. Raab and R. G. Cooks, *J. Chem. Educ.*, 2016, **93**, 340–344.
- W.-K. Rhim and S. K. Chung, *Methods*, 1990, **1**, 118–127.
- D. K. Bwambok, M. M. Thuo, M. B. J. Atkinson, K. A. Mirica, N. D. Shapiro and G. M. Whitesides, *Anal. Chem.*, 2013, **85**, 8442–8447.
- E. A. Crawford, C. Esen and D. A. Volmer, *Anal. Chem.*, 2016, **88**, 8396–8403.
- A. Marzo, A. Barnes and B. W. Drinkwater, *Rev. Sci. Instrum.*, DOI:10.1063/1.4989995.
- C. L. Heald, A. H. Goldstein, J. D. Allan, A. C. Aiken, E. Apel, E. L. Atlas, A. K. Baker, T. S. Bates, A. J. Beyersdorf, D. R. Blake, T. Campos, H. Coe, J. D. Crouse, P. F. DeCarlo, J. A. De Gouw, E. J. Dunlea, F. M. Flocke, A. Fried, P. Goldan, R. J. Griffin, S. C. Herndon, J. S. Holloway, R. Holzinger, J. L. Jimenez, W. Junkermann, W. C. Kuster, A. C. Lewis, S. Meinardi, D. B. Millet, T. Onasch, A. Polidori, P. K. Quinn, D. D. Riemer, J. M. Roberts, D. Salcedo, B. Sive, A. L. Swanson, R. Talbot, C. Warneke, R. J. Weber, P. Weibring, P. O. Wennberg, D. R. Worsnop, A. E. Wittig, R. Zhang, J. Zheng and W. Zheng, *Atmos. Chem. Phys.*, 2008, **8**, 2007–2025.
- S. K. Friedlander, *Aerosol Sci. Technol.*, 1982, **1**, 3–13.
- E. R. Duranty, S. A. Jacoby and J. H. Davis Jr., in *ECS Transactions of the 234th Meeting of the ECS*, 2018.
- B. Leckner, *Combust. Flame*, 1972, **19**, 33–48.
- C. A. Schneider, W. S. Rasband and K. W. Eliceiri, *Nat. Methods*, 2012, **9**, 671–675.
- O. C. Bridgeman and E. W. Aldrich, *J. Heat Transfer*, 1964, **86**, 279–286.
- H. C. Van NESS, C. A. Soczek1, G. L. Peloquin and R. L. Machado, *J. Chem. Eng. Data*, 1967, **12**, 217–224.
- H. F. Gibbard and J. L. Creek, *J. Chem. Eng. Data*, 1974, **19**, 308–310.
- C. N. Davies, in *Fundamentals of Aerosol Science*, ed. D. T. Shaw, Wiley-Interscience, 1978, pp. 135–164.
- S. C. Gibson, C. S. Feigerle and K. D. Cook, *Anal. Chem.*, 2014, **86**, 464–472.
- L. Tang and P. Kebarle, *Anal. Chem.*, 1993, **65**, 3654–3668.